



# Si allotropes and group IV clathrates investigated under high pressures

Duck Young Kim<sup>1,2\*</sup> and Tetsuji Kume<sup>3\*</sup>

HPSTAR  
363-2017

<sup>1</sup>Center for High Pressure Science and Technology Advanced Research, Shanghai 201203, China

<sup>2</sup>Geophysical Laboratory, Carnegie Institution of Washington, Washington, D.C. 20015, U.S.A.

<sup>3</sup>Department of Electrical, Electronic and Computer Engineering, Faculty of Engineering, Gifu University, Gifu 501-1193, Japan

\*E-mail: duckyoung.kim@hpstar.ac.cn; kume@gifu-u.ac.jp

Received November 14, 2016; accepted December 27, 2016; published online April 13, 2017

Recent studies on new materials crystallized with the  $sp^3$  open framework of Si and other group IV elements are reviewed. The synthesis and predicted properties of a new allotrope of silicon, i.e., orthorhombically structured silicon  $Si_{24}$ , are investigated.  $Si_{24}$  can be formed by heating a  $Na_4Si_{24}$  precursor at temperatures as low as 47 °C. The quasi-direct band-gap nature with a gap of  $\sim 1.3$  eV is predicted on the basis of a first-principles calculation. We also review investigations on clathrate materials having Si, Ge or Sn framework atoms for which pressure plays an important role. The phenomena and characteristics of clathrates under high pressures, i.e., the volume collapse phase transition and amorphization, are discussed on the basis of a survey over various clathrates with types I, II, III, and VIII structures.

© 2017 The Japan Society of Applied Physics

## 1. Introduction

The importance of silicon to our contemporary technology cannot be overemphasized as illustrated in the simple statement “carbon gives biology, but silicon gives geology and semiconductor technology”.<sup>1)</sup> Silicon is one of the most studied elements and its physical drawback is also well known; silicon is a semiconductor with an indirect band gap (1.12 eV), resulting in its physical limits for integrated transistors, and its direct band gap (3.2 eV) is beyond the visible light range, making it inefficient for photovoltaic applications.<sup>2–4)</sup>

Silicon is a mainstay of contemporary semiconducting science and technology, which rely on its abundance, high thermodynamic stability, and existence of a compatible dioxide,  $SiO_2$ . Silicon is the second abundant element on Earth, and diamond-structured silicon (d-Si) is the most stable form over wide ranges of pressures and temperatures. Establishing the phase diagram of silicon has led us to a few metastable forms of silicon stabilized under ambient conditions out of the existing thirteen allotropes. Two metastable forms of silicon with  $sp^3$  bonding were reported for Si-III in 1964<sup>5)</sup> and for Si-IV in 1963.<sup>6)</sup> However, they did not improve the required physical property beyond d-Si.

There have been many efforts over the past few decades to overcome the indirect gap limitations of d-Si and find alternative solutions. Silicon alloys with isoelectronic germanium,  $Si_{1-x}Ge_x$ , exhibit band gaps that are tunable by changing  $x$ ;<sup>7)</sup> however, these alloys generally retain an indirect band structure. A recent computational study involving the search for genetic algorithms suggested that a superstructure of  $SiGe_2Si_2Ge_2SiGe_n$  presents direct and dipole-allowed transitions.<sup>8)</sup> However, the growth of this superstructure would require extremely precise control over the exact composition that dictates the ultimate band structure. Ternary systems such as  $(Ge_2)_x(GaAs)_{1-x}$  and  $CuIn(P/Se)_2$  show improved performance as optoelectronic devices over silicon, but they are subject to phase separation.<sup>9)</sup> Theoretical studies of  $Si_{34-x}Ge_x$  clathrate alloys<sup>10)</sup> have predicted a range of values for the band gap (1.2–2 eV) and direct band gap for particular values of  $x$ . These compositions, however, have not yet been experimentally synthesized. The structural complexity, experimental chal-

lenges, and/or thermodynamic stability of the aforementioned materials, combined with the advantages of Si for the electronics industry, have led to the reinvigoration of pure silicon research.<sup>3,4,11–14)</sup>

The phase diagram of silicon has been extensively studied and more than 13 allotropes of silicon have been reported. Si-I (d-Si) has a cubic diamond structure and a thermodynamic ground state under ambient conditions. Si-III (cB8 or commonly known as “BC8”), Si-IV (lonsdaleite, hP4), and Si-XII (hR8 or commonly known as “R8”) are all metastable structures produced by decompressing stable phases from high pressure.<sup>15)</sup> The BC8 structure is likely semimetallic<sup>16)</sup> and the R8 structure was calculated to show a small indirect gap of 0.24 eV.<sup>17)</sup> Lonsdaleite is produced by heating the BC8 structure above 470 K and has an indirect gap of  $\sim 1$  eV.<sup>16,17)</sup> Additionally,  $Si_{136}$ , which is a modified type-II silicon clathrate that is free of “guest” atomic species,<sup>18)</sup> and *allo*-Si<sup>19)</sup> may be considered as two other silicon allotropes. However,  $Si_{136}$  shows a wide band gap of 1.9 eV<sup>18,20)</sup> and the crystal structure of *allo*-Si is not clearly resolved.<sup>21)</sup>

Among the Si allotropes and Si-related materials, clathrate materials with guest atoms have been extensively investigated so far because of their distinct properties that address their important thermoelectric, phonon, and glass-related electronic issues,<sup>22,23)</sup> as well as their superconductivity.<sup>24,25)</sup> These novel properties originate from the interaction between the host framework and the guest species included in the clathrate open structure. The host–guest interaction also affects the structural stability, leading to unique phenomena under high pressures, i.e., the isostructural volume collapse phase transition and reversible amorphization.

In this article, we review high-pressure studies on Si-related materials, namely, *allo*-Si and group IV clathrates. This article is organized as follows: In Sect. 2 we describe the synthesis and properties of the new Si allotrope  $Si_{24}$  using high pressure.<sup>26)</sup> The high-pressure behaviors of clathrates of Si, Ge, and Sn are described in Sect. 3. A summary of the recent research studies of *allo*-Si and group IV clathrates is shown in Sect. 4.

## 2. Synthesis and properties of a new Si allotrope under high pressure

Originally, we were interested in high-pressure behaviors of

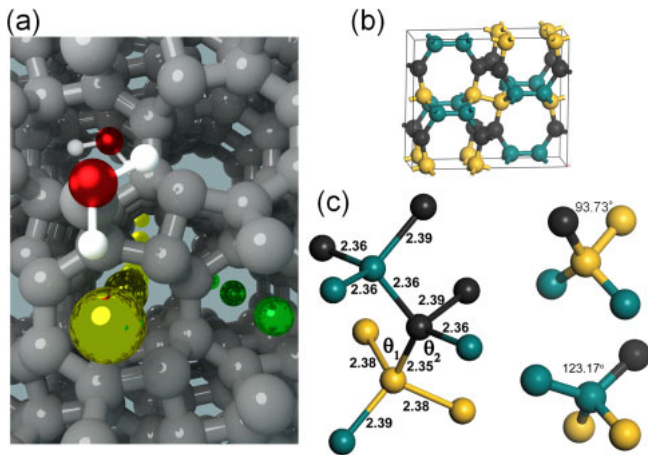


**Fig. 1.** (Color online) Schematic view of the crystal structure of  $\text{Si}_{24}$ . (a)  $\text{Si}_{24}$  framework (grey) with penetrating metal atoms and molecules, emphasizing its porosity. (b) Conventional unit cell of  $\text{Si}_{24}$  with three different symmetric sites in different colors. (c) Part of the unit cell in  $\text{Si}_{24}$  showing the bond lengths in angstrom units and the bond angles.

metal silicon clathrates to test if they are thermodynamically stable phases under extreme compression. We pressurized the Na/Si mixture up to 10 GPa, and we found an unprecedented form of the Na–Si compound, namely,  $\text{NaSi}_6$ ,<sup>27</sup> stabilized thermodynamically.  $\text{NaSi}_6$  ( $\text{Na}_4\text{Si}_{24}$  in the conventional unit cell) possesses a  $\text{Eu}_4\text{Ga}_8\text{Ge}_{16}$  type structure, which consists of  $\text{sp}^3$ -bonded Si and interpenetrating Na atoms. An equivalent structure was also reported in  $\text{BaSi}_6$ ,<sup>28</sup>  $\text{SrSi}_6$ ,<sup>29</sup>  $\text{CaSi}_6$ ,<sup>30</sup> and  $\text{EuSi}_6$ .<sup>31</sup> We report here the synthesis of a new allo-Si and its properties predicted on the basis of first-principles calculation. The electronic structure calculations were performed using the density functional theory (DFT)<sup>32,33</sup> with the generalized gradient approximation (GGA)<sup>34</sup> of Perdew–Burke–Ernzerhof (PBE)<sup>35</sup> used for the exchange–correlation functional, which was implemented by means of the same algorithm package indicated in Ref. 36. We used a plane-wave basis set with a cutoff at 500 eV and a uniform Brillouin-zone sampling of  $16 \times 16 \times 16$  k-points for  $\text{Si}_{24}$  and  $6 \times 6 \times 6$  for  $\text{Si}_{136}$ . To estimate the band gap correctly, we supplemented these calculations by employing the Bethe–Salpeter equation (BSE)<sup>37,38</sup> to compute the Coulomb correlation between photoexcited electrons and holes using ABINIT software.<sup>39</sup>

$\text{Na}_4\text{Si}_{24}$  exists under ambient conditions as a metastable form and it was also observed that we can evaporate Na atoms by raising the temperature to as low as 320 K. The gradual release of Na atoms into other guest–host-type silicon case structures was reported; however, it requires a much higher temperature. For example, type-II silicon clathrate ( $\text{Na}_x\text{Si}_{136}$ ) showed similar phenomena near 623 K<sup>20,40</sup> and we speculate that this difference is closely related to the geometry of the systems because Na atoms form linear chains in  $\text{Na}_4\text{Si}_{24}$  while Na atoms are captured in  $\text{Na}_x\text{Si}_{136}$ . Owing to the strong  $\text{sp}^3$  covalent bond nature of Si atoms, the framework is still maintained without Na atoms, forming an allotrope of silicon, namely,  $\text{Si}_{24}$ .<sup>26</sup> In Fig. 1, we show a schematic view of the crystal structure of  $\text{Si}_{24}$ . The Si–Si bond length ranges from 2.35 to 2.39 Å and the bond angle is strongly distorted, varying between the smallest angle  $\theta_1$  ( $93.73^\circ$ ) and the largest angle  $\theta_2$  ( $123.17^\circ$ ) compared with the

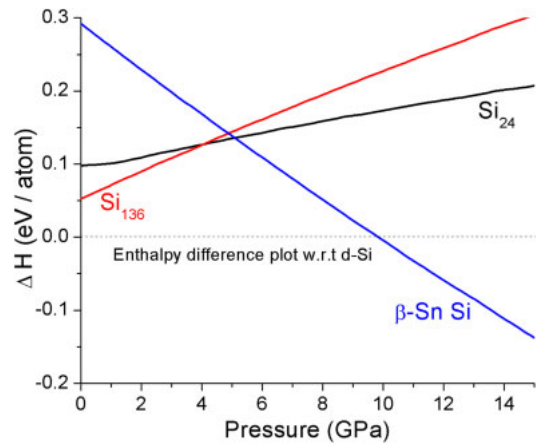


**Fig. 2.** (Color online) Comparison of total energies of several silicon phases with respect to pressure.

ideal angle ( $109.5^\circ$ ). Note that  $\text{Si}_{24}$  is thermodynamically stable against temperature and pressure, comparable to d-Si despite the distorted bonds. In our report,<sup>26</sup> we showed that  $\text{Si}_{24}$  was observed to be stable up to  $\sim 723$  K in experiments, and harmonic phonon calculations predicted that  $\text{Si}_{24}$  can exist up to 10 GPa.

Figure 2 shows a comparison of the total energies of several Si structures with respect to d-Si. Along the thermodynamic path, the phase transition from d-Si to  $\beta$ -tin-structured Si ( $\beta$ -Sn Si) is predicted at  $\sim 10$  GPa, which is consistent with the well-known phase boundary of silicon.<sup>41</sup> At ambient pressure, the total energy of  $\text{Si}_{24}$  is higher than that of d-Si by  $\sim 0.09$  eV/atom, while the well-known  $\text{Si}_{136}$  exhibits a lower energy than  $\text{Si}_{24}$ .  $\beta$ -Sn Si appears to be much higher in total energy at ambient pressure by  $\sim 0.29$  eV/atom and it becomes the ground state above 10 GPa. We speculate that an energy difference within 0.1 eV/atom in  $\text{sp}^3$  bonded silicon phases can be safely stabilized regardless of bond length/angle deviation from the ideal d-Si.

The electronic band structure of  $\text{Si}_{24}$  reveals a marked change in band structure compared with that of d-Si. Although d-Si shows a direct band gap ( $E_d$ ) of  $\sim 3.2$  eV and an indirect band gap ( $E_i$ ) of  $\sim 1.12$  eV,  $\text{Si}_{24}$  possesses a quasi-direct band gap nature, indicating both  $E_d$  and  $E_i$  band gaps of 0.57 and 0.53 eV, respectively, in standard DFT calculations as shown in Fig. 3. It is a well-known problem of standard DFT calculations that the band gaps of most semiconductors are underestimated; thus, we also performed quasiparticle calculations (GW) to obtain the appropriate band gap. GW calculations rigidly shift bands near the Fermi level and  $E_d$  and  $E_i$  become 1.34 and 1.30 eV, respectively. The difference between  $E_d$  and  $E_i$  in d-Si is  $\sim 2$  eV and now it is reduced to  $< 0.1$  eV, forming a quasi-direct band gap.

As  $\text{Si}_{24}$  is a quasi-direct-band-gap semiconductor with 1.3 eV, we also examined a potential application for photovoltaics. The imaginary dielectric function ( $\epsilon_2$ ) can be seen as a good measure of the solar spectral energy absorption of semiconductors. By solving the BSE for the allotropes of silicon (d-Si,  $\text{Si}_{24}$ , and  $\text{Si}_{136}$ ), we could predict how  $\text{Si}_{24}$  improves solar spectral absorption. As shown in Fig. 4, the  $\epsilon_2$  of three silicon allotropes has a finite amplitude in the visible light range 1.6 (red)–3.2 (violet) eV. Owing to the lack of the direct transition of d-Si below 3.2 eV, the amplitude remains

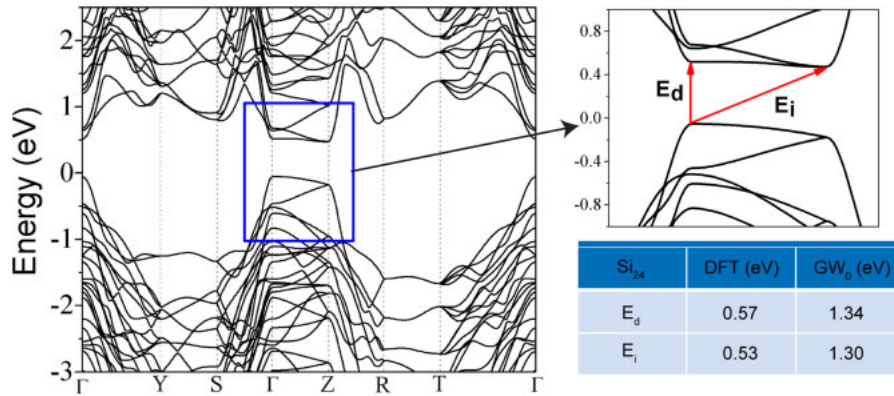


Fig. 3. (Color online) Calculated electronic band structure of Si<sub>24</sub> using standard DFT. The gap energies for the DFT and GW are presented.

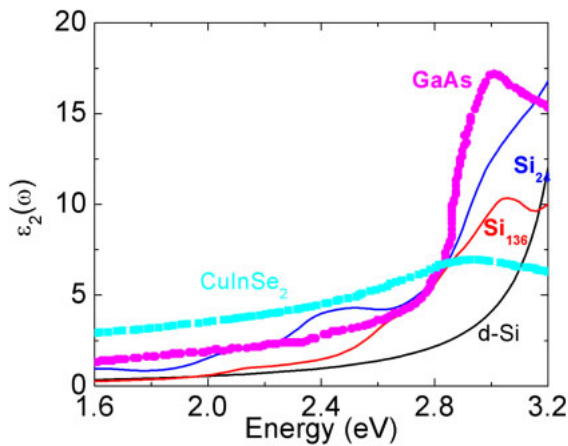


Fig. 4. (Color online) Calculated solar spectral absorptions of d-Si, Si<sub>24</sub>, Si<sub>136</sub>, GaAs, and CuInSe<sub>2</sub>.

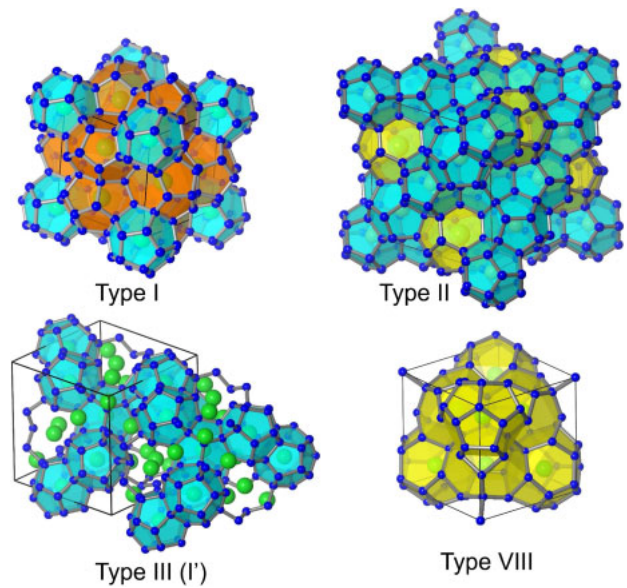


Fig. 5. (Color online) Crystal structures of typical clathrates, types I, II, III (I'), and VIII.

small, which is regarded as the fundamental limitation of d-Si as a photovoltaic material. However, Si<sub>136</sub> and Si<sub>24</sub> exhibit enhanced amplitudes and, furthermore, especially as a single element, Si<sub>24</sub> shows a compatible performance with GaAs,<sup>42</sup> which has a higher efficiency for photovoltaics. Also, note that optical absorption in Si<sub>24</sub> starting from the absorption edge is dipole-allowed, while dipole transition in cubic-structured Si<sub>136</sub> is forbidden.

### 3. Group IV clathrates under high pressure

#### 3.1 Structure of group IV clathrates

For clathrate materials having a polyhedron cage, several types of structures have been well known. The typical structures are shown in Fig. 5 and their crystal data are summarized in Table I. Since the structures and synthesis have been described in detail elsewhere,<sup>43–46</sup> brief explanations are presented here. The most common forms in the clathrates are known as types I and II, which are isostructural with hydrogen-bonded H<sub>2</sub>O clathrates.<sup>47,48</sup>

The type-I structure with the space group  $Pm\bar{3}m$  is formed by two highly symmetric E<sub>20</sub> dodecahedra and six E<sub>24</sub> tetrakaidecahedra in a cubic unit cell connected by face sharing, which can be represented by the general formula of M<sub>8</sub>E<sub>46</sub> if host E cages are fully occupied by guest atoms M. The host E atoms are basically of group IV elements (Si, Ge, Sn), but the group III (Ga, Al) or group V (Sb) atoms can partially substitute for them, leading to ternary or quaternary

clathrates such as Ba<sub>8</sub>Ga<sub>16</sub>Ge<sub>16</sub>.<sup>49,50</sup> The 6c site in the type-I structure tends to form vacancies. The typical example is Ba<sub>8</sub>Ge<sub>43</sub>[...]<sub>3</sub>, which has three defects on the 6c site, making Ge atoms at the neighboring site (24k site) three-bonded.<sup>51–53</sup> The type-II structure with the space group  $Fd\bar{3}m$  is formed by 16 E<sub>20</sub> and eight E<sub>28</sub> cages connected by face sharing in its cubic unit cell. The full occupation of the guest M atoms corresponds to the formula of M<sub>24</sub>E<sub>136</sub>. Off-stoichiometric M<sub>x</sub>E<sub>136</sub> (0 < x < 24) is also stable.

The type-III clathrate (expressed also as Type I') is formulated as M<sub>24</sub>E<sub>100</sub>.<sup>54,55</sup> The cubic structure with the space group  $P4_132$  is constructed with spirally chained E<sub>20</sub> cages and many three-bonded E atoms. The guest M atoms occupy the interstitial sites and the sites inside the E<sub>20</sub> cages, as shown in Fig. 1.

The type-VIII clathrate with non-centrosymmetrical  $I\bar{4}3m$  takes the same stoichiometry (M<sub>8</sub>E<sub>46</sub>) as the type I. The structure consists of only one type of polyhedral cage centered by an M atom (8c site) in contrast to the two types of cage in the type-I clathrate. The type-VIII host structure has four Wyckoff positions (2a, 8c, 12d, and 24g) occupied by the E atoms of the framework. This structure has been observed for ternary or quaternary clathrates.

**Table I.** Composition and structural parameters of type-I, type-II, type-III, and type-VIII clathrates of group IV elements.

	Type I	Type II	Type III	Type VIII
Main formulae	$M_xE_{46}$ ( $6 < x < 8$ )	$M_xE_{136}$ ( $0 < x < 24$ )	$M_{24}E_{100}$	$M_8E_{46}$
Examples				
Binary	$Ba_8Si_{46}$ , $K_8Si_{46}$	$Na_1Si_{136}$	$Ba_{24}Si_{100}$ , $Ba_{24}Ge_{100}$	
Ternary	$Ba_8Ga_{16}Ge_{30}$			$Ba_8Ga_{16}Ge_{30}$
Quaternary	$Sr_8Al_7Ga_9Si_{30}$			$Sr_8Al_8Ga_8Si_{30}$
Defect	$Ba_8Ge_{43}$			
Space group	$Pm\bar{3}n$ (No. 223)	$Fd\bar{3}m$ (No. 227)	$P4_32$ (No. 213)	$I\bar{4}3m$ (No. 217)
Typical M atomic positions	2a (0, 0, 0) 6d (0.25, 0.5, 0)	8b (3/8, 3/8, 3/8) 16c (0, 0, 0)	8c (0.19, 0.19, 0.19) 4b (7/8, 7/8, 7/8) 12d (1/8, 0.810, 0.060)	8c (0.186, 0.186, 0.186)
Typical E atomic positions	6c (0.25, 0, 0.5) 16i (0.183, 0.183, 0.183) 24k (0.31, 0.116, 0.31)	8a (7/8, 7/8, 7/8) 32e (0.782, 0.782, 0.782) 96g (0.817, 0.817, 0.6285)	8c (0.0305, 0.0305, 0.0305) 24e (0.203, 0.043, 0.00) 12d (1/8, 0.169, 0.419) 24e (0.240, 0.935, 0.874) 24e (0.416, 0.853, 0.083) 8c (0.325, 0.325, 0.325)	2a (0, 0, 0) 8c (0.365, 0.365, 0.365) 12d (0.25, 0.5, 0) 24g (0.416, 0.416, 0.144)

### 3.2 $Sr_8Al_xGa_ySi_{30}$ clathrates

We present here the high-pressure X-ray diffraction (XRD) and Raman study of the type-VIII clathrate. Quaternary clathrates of  $Sr_8Al_xGa_{16-x}Si_{30}$  are known to take both the type-I and type-VIII structures depending on the composition of Al and Ga; the Ga-rich ( $0 < x < 7$ ) and Al-rich ( $8 < x < 13$ ) conditions lead to types I and VIII, respectively.<sup>56</sup> To compare the high pressure behaviors between the type-I and type-VIII clathrates, we have carried out the high pressure XRD and Raman measurements of the type-VIII ( $Sr_8Al_7Ga_9Si_{30}$ ) and type-I ( $Sr_8Al_8Ga_8Si_{30}$ ) clathrates. The samples of  $Sr_8Al_7Ga_9Si_{30}$  (type I) and  $Sr_8Al_8Ga_8Si_{30}$  (type VIII) prepared by spark plasma sintering (SPS)<sup>56</sup> were placed in a diamond anvil cell (DAC) with a culet of 0.3 mm diameter for high-pressure XRD and Raman experiments. Each sample was cut and polished into a plate of  $\sim 50 \mu\text{m}$  size and  $\sim 20 \mu\text{m}$  thickness. The sample was loaded into the DAC with an Ar pressure medium. Raman spectra were measured using a spectrometer equipped with a triple-grating monochromator and a charge coupled-device detector. A solid state laser with a wavelength of 532 nm was used for excitation. Pressure calibration was carried out by the ruby method.

Figures 6(a)–6(d) show results of XRD and Raman measurements for  $Sr_8Al_7Ga_9Si_{30}$  (type I) and  $Sr_8Al_8Ga_8Si_{30}$  (type VIII) clathrates under high pressures up to 30 GPa. For the type-I clathrate, the XRD pattern [Fig. 6(b)] showed a marked change at  $P \simeq 18$  GPa, and the pattern then gradually became amorphous without distinct peaks, which is well consistent with the change from a Raman spectrum to an amorphous spectrum above 18 GPa [Fig. 6(a)]. At pressures  $P < 16$  GPa, all of the XRD peaks were well indexed with the primitive cubic structure ( $Pm\bar{3}n$ ). At  $P = 18$  GPa, almost all the peaks were fitted well with the cubic symmetry, but slight deviations were found between the observed and calculated peak positions of, e.g., the (400) and (410) reflections. Therefore, a structure transformation into a non-cubic system occurs at 16 GPa. The same type of deviation

from the cubic system has been reported for the high-pressure phase of the type-I clathrate  $Ba_8Ga_{16}Ge_{30}$ .<sup>57</sup> According to the previous paper, a tetragonal or orthorhombic distortion occurs in the quasi-cubic phase. In Fig. 7(a), the pressure dependence of the  $Sr_8Al_7Ga_9Si_{30}$  cell volume is presented (solid circles). The cell volume of the quasi-cubic phase was tentatively obtained by assuming that the strongest diffraction peak was the (321) reflection of the cubic unit cell. A jump is observed at 14 GPa in the compression curve, which can be assigned to the volume collapse transition.

For type VIII [Fig. 6(d)], the XRD pattern did not show a distinct change up to  $P \sim 20$  GPa, but all of the peaks gradually disappeared at  $P > 20$  GPa, leading to an amorphous pattern. Raman spectra also changed to be amorphous. XRD peak positions were well explained by the cubic system ( $Pm\bar{3}n$ ) up to around 25 GPa. In Fig. 7(a) (solid squares), the unit cell volume normalized with that at 1 atm is plotted as a function of pressure. An abrupt jump is found at 20 GPa in spite of the absence of structural change. Thus, we see that the isostructural volume collapse transition occurs also for the type-VIII clathrate.

For both type-I and type-VIII clathrates, the amorphization is strongly suggested by the features of XRD patterns and Raman spectra. When the pressure was released from 29.8 GPa, however, the XRD patterns were reversibly changed, as shown in the upper panels of Figs. 6(b) and 6(d). The XRD profiles after compression have broad backgrounds riding under the sharp peaks, implying that there are regions of the sample where the long-range order has not been restored. This type of reversible change, i.e., the reversible amorphization, has been observed also for other clathrates.<sup>57,58</sup> However, all the previous cases were observed for type-I clathrates. Thus, the reversible amorphization observed here for  $Sr_8Al_8Ga_8Si_{30}$  is the first case of the type-VIII clathrate.

### 3.3 Phase transition and amorphization of clathrates

A high pressure study of group IV clathrates was performed by San-Miguel et al. for the first time on the type-II Si

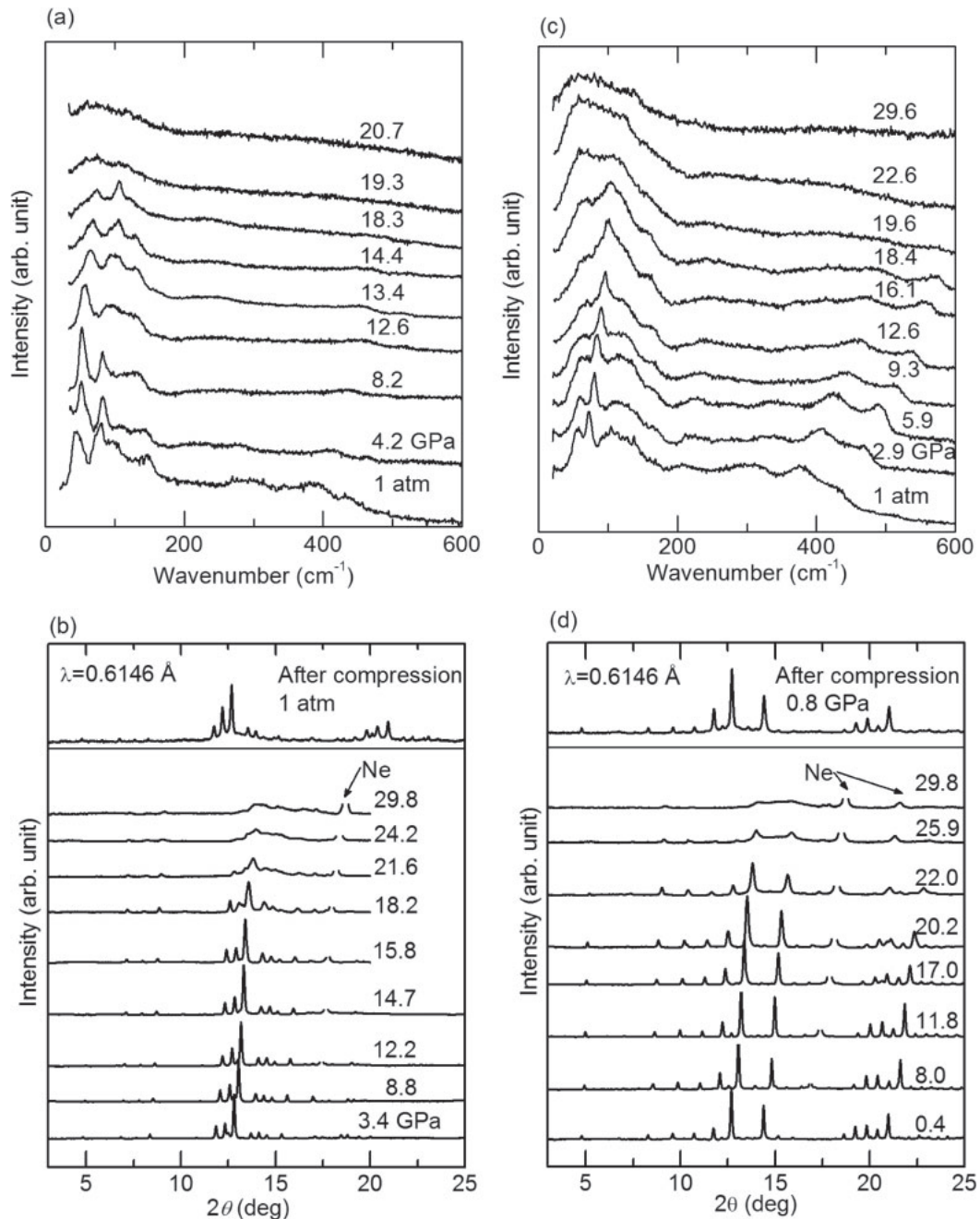


**Fig. 6.** Raman and XRD experimental data of  $\text{Sr}_8\text{Al}_7\text{Ga}_9\text{Si}_{30}$  (type I) and  $\text{Sr}_8\text{Al}_8\text{Ga}_8\text{Si}_{30}$  (type VIII) measured under high pressures: (a) Raman of  $\text{Sr}_8\text{Al}_7\text{Ga}_9\text{Si}_{30}$  (type I), (b) XRD of  $\text{Sr}_8\text{Al}_7\text{Ga}_9\text{Si}_{30}$  (type I), (c) Raman of  $\text{Sr}_8\text{Al}_8\text{Ga}_8\text{Si}_{30}$  (type VIII), and (d) XRD of  $\text{Sr}_8\text{Al}_8\text{Ga}_8\text{Si}_{30}$  (type VIII).

clathrate ( $\text{Na}_1\text{Si}_{136}$ ) that was almost free of guest Na.<sup>59)</sup> This material transforms to a  $\beta$ -Sn structure at the same pressure of 11.5 GPa as does the d-Si.<sup>60)</sup> Since then, various clathrates of Si,<sup>59,61–73)</sup> Ge,<sup>57,58,74–76)</sup> and Sn<sup>77,78)</sup> have been investigated under high pressures. Table II shows a list of the phase transition pressures, and Figs. 7(a) and 7(b) include the compression curves reported for Si and Ge clathrates, respectively. For comparison, the data of diamond-structured Si and Ge are also indicated in Table II and Fig. 7.<sup>60,79,80)</sup> Note that the type-I clathrates with full guest occupation show different high-pressure behaviors from d-Si.<sup>60,79)</sup> For example, the type-I  $\text{Ba}_8\text{Si}_{46}$  undergoes two phase transitions at 6 and 13 GPa, and amorphization at 40 GPa. The Raman spectra are observed to change at 6 GPa without a change in structure.<sup>64)</sup> The 13 GPa transition causes an abrupt decrease

in unit cell volume [see open squares in Fig. 7(a)] without a change in XRD pattern. This isostructural-volume-collapse transition was firstly observed by San-Miguel et al.<sup>62)</sup> Both transitions have been explained in terms of changes in electronic topology caused by charge transfer between the guest Ba and the host Si.<sup>63,65–67)</sup>

The volume collapse phase transition observed for  $\text{Ba}_8\text{Si}_{46}$  has been commonly observed for other type-I clathrates ( $\text{K}_8\text{Si}_{46}$ ,<sup>69,70)</sup>  $\text{Rb}_{6.15}\text{Si}_{46}$ ,<sup>71)</sup>  $\text{I}_8\text{Si}_{44}\text{I}_2$ ,<sup>61)</sup>  $\text{Sr}_8\text{Al}_7\text{Ga}_9\text{Si}_{30}$ ,  $\text{Ba}_8\text{Ga}_{16}\text{Ge}_{30}$ ,<sup>57)</sup>  $\text{Sr}_8\text{Ga}_{16}\text{Ge}_{30}$ ,<sup>74)</sup>  $\text{Eu}_8\text{Ga}_{16}\text{Ge}_{30}$ ,<sup>75)</sup> and  $\text{I}_8\text{Sb}_8\text{Ge}_{38}$ <sup>74)</sup>) and the type-VIII clathrate  $\text{Sr}_8\text{Al}_8\text{Ga}_8\text{Si}_{30}$ . The transition pressures ( $P_3$ ) are listed in Table II. Further pressurization often causes the amorphization. The reversibility of the amorphization was identified for several clathrates, as presented here on the type-I ( $\text{Sr}_8\text{Al}_7\text{Ga}_9\text{Si}_{30}$ )

**Table II.** Phase transition and amorphization pressures of group IV clathrates.  $P_1$ ,  $P_3$ , and  $P_4$  correspond to the transition pressures of the isostructural transition without volume change, the volume collapse transition, and the amorphization transition, respectively.  $P_2$  corresponds to the phase transition to the  $\beta$ -Sn structure. The right column represents reversibility. Namely, “Y” denotes a structure recovered after applying the pressure indicated in parentheses.

Str type		Isostructural $P_1$ (GPa)	$P_2$ (GPa)	Vol. collapse $P_3$ (GPa)	Amorphization $P_4$ (GPa)	Reversibility
Diamond	Si		11.5			
II	Na <sub>1</sub> Si <sub>136</sub>		11.5			
I	Na <sub>8</sub> Si <sub>46</sub>		13			N
I	Ba <sub>8</sub> Si <sub>46</sub>	6		13	40	Y (20 GPa) N (49 GPa)
I	K <sub>8</sub> Si <sub>46</sub>	6.5		23	32	
I	Rb <sub>6.15</sub> Si <sub>46</sub>	13		24	30	Y (15 GPa) N (36 GPa)
I	Ba <sub>8</sub> Ag <sub>6</sub> Si <sub>40</sub>			28		
I	I <sub>8</sub> Si <sub>44</sub> I <sub>2</sub>			35	47	
III (I')	Ba <sub>24</sub> Si <sub>100</sub>	6.5			23	N (27 GPa)
VIII	Sr <sub>8</sub> Al <sub>8</sub> Ga <sub>8</sub> Si <sub>30</sub>			20	26	Y (30 GPa)
I	Sr <sub>8</sub> Al <sub>7</sub> Ga <sub>9</sub> Si <sub>30</sub>			14	22	Y (30 GPa)
Diamond	Ge		10.6			
I	Ba <sub>8</sub> Ga <sub>16</sub> Ge <sub>30</sub>			33	35	Y (41 GPa)
I	Sr <sub>8</sub> Ga <sub>16</sub> Ge <sub>30</sub>			19	20	Y (21 GPa)
I	Eu <sub>8</sub> Ga <sub>16</sub> Ge <sub>30</sub>			13	14	
I	I <sub>8</sub> Sb <sub>8</sub> Ge <sub>38</sub>			41	36–44	N (50 GPa)
I	Ba <sub>8</sub> Ge <sub>43</sub> [...] <sub>3</sub>				37	Y (41 GPa)
III (I')	Ba <sub>8</sub> Ge <sub>100</sub>	6			22	N (26 GPa)
Diamond	Sn		0.9			
I	Ba <sub>8</sub> Ga <sub>16</sub> Sn <sub>30</sub>				6.2	N (6.2 GPa)
I	Rb <sub>8</sub> Sn <sub>44</sub> [...] <sub>2</sub>				7.9	

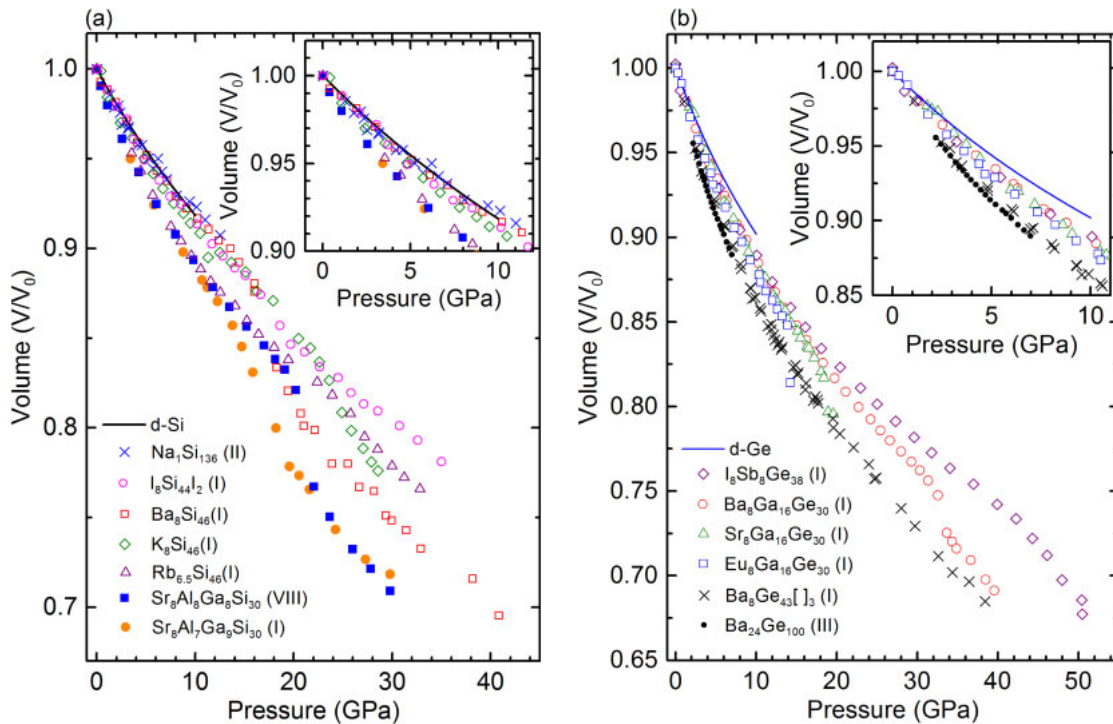


**Fig. 7.** (Color online) Pressure dependence of unit cell volume normalized by that under ambient condition: (a) Si- and (b) Ge-related materials.

and type-VIII (Sr<sub>8</sub>Al<sub>8</sub>Ga<sub>8</sub>Si<sub>30</sub>) clathrates. The amorphization of the clathrate will be discussed later.

As noted in Fig. 7(b) and Table II, the reversible amorphization transition, but no volume collapse transition, was observed for Ba<sub>8</sub>Ge<sub>43</sub>[...]<sub>3</sub>, in which there are vacancies on the 6c site of the type-I structure.<sup>58)</sup> This implies that the 6c site plays an important role in the volume-collapse

transition. To gain insight into the role of the 6c site in the volume-collapse transition, the atomic positions of Ba<sub>8</sub>Ga<sub>16</sub>Ge<sub>30</sub> have been investigated under high pressures.<sup>57)</sup> Figure 8(a) shows the pressure dependence of the internal coordinates of the host atoms obtained from the Rietveld refinement of XRD data of Ba<sub>8</sub>Ga<sub>16</sub>Ge<sub>30</sub>.<sup>57)</sup> Since the internal atomic coordinates for the type-I clathrate are (0, 0, 0) for

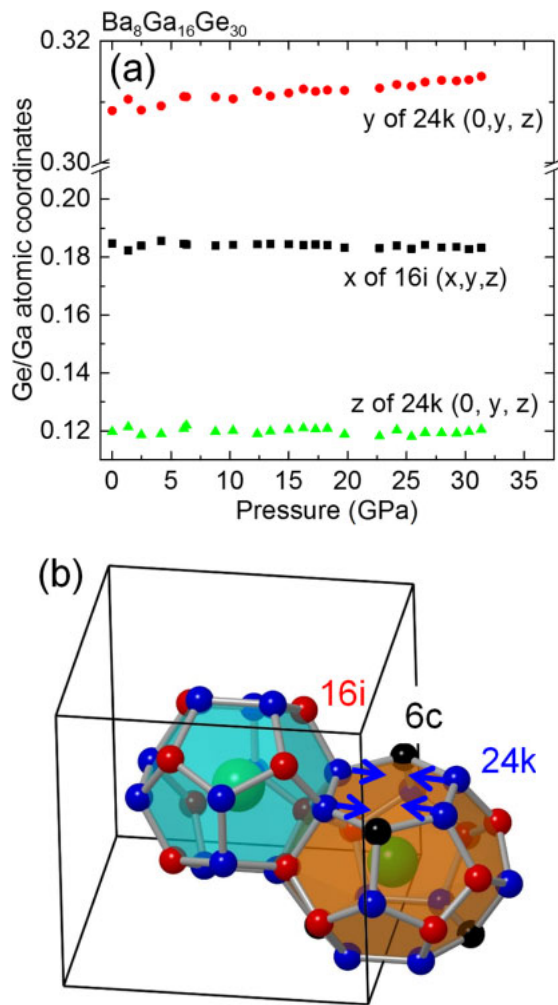


**Fig. 8.** (Color online) (a) Pressure dependence of internal atomic coordinate parameters obtained for  $\text{Ba}_8\text{Ga}_{16}\text{Ge}_{30}$ .<sup>57)</sup> (b) Small and large cages of  $\text{Ba}_8\text{Ga}_{16}\text{Ge}_{30}$ . The unit cell is represented by a cube drawn by solid lines. The Wyckoff sites (6c, 16i, and 24k) of the host atoms are indicated. Arrows show the displacements for the 24k site induced by pressurization.

Ba(2a), (0.25, 0.5, 0) for Ba(6d), (0.25, 0, 0.5) for Ge/Ga(6c), (x, x, x) for Ge/Ga(16i), and (0, y, z) for Ge/Ga(24k), there are three parameters for the atomic coordinates y and z for the 24k site and x for the 16i site. As seen in this figure, only the y coordinate of the 24k site slightly increased with increasing pressure up to the transition, while the others almost remained constant. This implies that some parts of the structure are favorably shrinking when the crystal is compressed. In Fig. 8(b), the displacements of the 24k atoms are shown using arrows, according to the results in Fig. 8(a). These displacements give rise to the deformation of the hexagonal ring in the large cage. The same deformation of the hexagonal ring was reported also for  $\text{I}_8\text{Sb}_8\text{Ge}_{38}$ .<sup>74)</sup>

The scenario of the volume collapse transition followed by amorphization has been discussed in Ref. 57. First, the hexagonal ring is deformed under a high pressure. The 6c atoms are largely displaced from the initial position [Fig. 8(b)]. This leads to a deformation of the large cage ( $E_{24}$ ). Simultaneously, the rotation and/or deformation of the small cages ( $E_{24}$ ) occurs because a 6c atom bridges the small cages. As a result, a highly distorted cage structure is realized. Therefore, the high-pressure phases after the collapse transition are observed in strongly disordered

**Table III.** Bulk moduli of group IV clathrates.

Str type		$B_0$ (GPa)	$B'$
Diamond	Si	99.9	3.8
II	$\text{Si}_{136}$	90	
I	$\text{Ba}_8\text{Si}_{46}$	93	
I	$\text{K}_8\text{Si}_{46}$	86	
I	$\text{Na}_8\text{Si}_{46}$	93	
I	$\text{I}_8\text{Si}_{44}\text{I}_2$	95	
I	$\text{Sr}_8\text{Al}_7\text{Ga}_9\text{Si}_{30}$	61.4	5.5
VIII	$\text{Sr}_8\text{Al}_8\text{Ga}_8\text{Si}_{30}$	60.2	5.1
Diamond	Ge	74.9	3
I	$\text{Ba}_8\text{Ga}_{16}\text{Ge}_{30}$	67.2	3.5
I	$\text{I}_8\text{Sb}_8\text{Ge}_{38}$	64.7	4.5
I	$\text{Ba}_8\text{Ge}_{43}[\cdots]_3$	52.8	3.4

structures, which move more easily to full amorphization with further increase in pressure up to the amorphization transition. From Table II, the reversibility of amorphization seems to depend on the materials. This can be explained as follows. The distorted structure can turn back the original structure when the applied pressure is not markedly high. There is a threshold pressure at which the structure does not recover even if the pressure is released. For example, the distorted structure for  $\text{Ba}_8\text{Si}_{46}$  is attained at 13 GPa, and the threshold for reversible amorphization is between 20 and 49 GPa.

The binary type-III (I') clathrate  $\text{Ba}_{24}\text{Ge}_{100}$  has been investigated by Nakano<sup>81)</sup> and Shimizu et al.<sup>76)</sup> through XRD and Raman measurements, respectively. This clathrate is just as compressible as the defect clathrate  $\text{Ba}_8\text{Ge}_{43}[\cdots]_3$ . This is explained by the fact that there are many Ge atoms bonding only three neighbors. The existence of three-coordinate Ge atoms yields flexibility in the structure, leading to a higher compressibility.

For the clathrates without defects, the compressibility or bulk modulus ( $B_0$ ) shows variety as seen in Fig. 7 and Table III. However, note that all of the clathrates showed smaller  $B_0$  values than the diamond structure even if the guest atoms fully occupy the cages. The binary clathrates such as  $\text{Ba}_8\text{Si}_{46}$  show a slightly smaller  $B_0$ , indicating that the existence of guest atoms does not cause the structure to be stiff. The ternary or quaternary clathrates show significantly lower  $B_0$  values. This is because the covalent bond between Si (or Ge) and the other element is more compressive than the Si-Si (or Ge-Ge) bond. Therefore,  $B_0$  is independent of the guest atom species, but is determined by the nature of the host framework. On the other hand, the phase transition pressure depends on the guest atom species, as noted in Table II. The  $\text{sp}^3$  diamond structures of Si, Ge, and Sn are transformed to the  $\beta$ -Sn structure at 11.5, 10.6, and 0.9 GPa, respectively, while the  $\text{sp}^3$  clathrate structure can be maintained up to 47, 44, and 8 GPa for Si, Ge, and Sn clathrates, respectively. The existence of the guest atoms preserves the  $\text{sp}^3$  network of the clathrate at a very high pressure.

#### 4. Conclusions

In this article, we reviewed the studies on new materials crystallized by the  $\text{sp}^3$  open framework of Si and other

group IV elements. In Sect. 2, we reported a discovery of a new allotrope of silicon. It is an orthorhombic-structured silicon, namely,  $\text{Si}_{24}$ , formed by treating a  $\text{Na}_4\text{Si}_{24}$  precursor.<sup>26)</sup> By heating  $\text{Na}_4\text{Si}_{24}$  at temperatures as low as 47 °C, we observed that Na ions can be released and eventually  $\text{Na}_x\text{Si}_{24}$  becomes a sodium-free state. In our experiment, we confirmed that the sodium concentration was below our laboratory detection limit, and more importantly, its electrical behavior was semiconducting, which is in excellent agreement with our first-principles calculations. Surprisingly, the measured and predicted band gaps of  $\text{Si}_{24}$  are  $\sim 1.3$  eV and the direct and indirect band gaps are almost the same, forming a quasi-direct band gap. Hence,  $\text{Si}_{24}$  can be assigned to be the fourteenth allotrope of silicon, which is a quasi-direct-band-gap semiconductor with an optimal band-gap for photovoltaic applications. Our first-principles calculations showed that it exhibits an improved solar absorption over d-Si. Moreover, its quasi-direct band-gap nature can potentially overcome the limitations of d-Si as light emitters<sup>4)</sup> and interband tunnel field-effect transistors.<sup>3)</sup>

In Sect. 3, the high-pressure studies carried out so far on group IV clathrates with types-I, II, III (I'), and VIII structures were summarized. The volume collapse isostructural phase transition firstly observed for  $\text{Ba}_8\text{Si}_{46}$  has been commonly found in other type-I clathrates and even in the type-VIII clathrate  $\text{Sr}_8\text{Ga}_8\text{Al}_8\text{Si}_{38}$ . However, there is no such phase transition in the defect type-I clathrate  $\text{Ba}_8\text{Ge}_{43}$  and in the type-III (I') clathrate having threefold-bonded Ge. Pressure-induced amorphization is also common in the type-I, type-III, and type-VIII clathrates. For some clathrates (types I and VIII), the crystalline phase was recovered after releasing pressure from the amorphous state. The amorphous state was discussed on the basis of the atomic displacement under high pressures, and understood as a highly distorted structure. Since the isostructural volume collapse and reversible amorphization are independent of the structure type in the clathrates, those transitions are likely to be common phenomena of the guest–host materials.

### Acknowledgments

D.Y.K. acknowledges the support of NSAF Grant No. U1530402 in China and the Energy Frontier Research in Extreme Environments (EFREE) Center, an Energy Frontier Research Center funded by the U.S. Department of Energy, Office of Science, Office of Basic Energy Science under Award No. DE-SC0001057. T.K. thanks Dr. K. Kishimoto, Dr. N. Ikeda, Professor T. Koyanagi of Yamaguchi University, Professor S. Yamanaka, Dr. H. Fukuoka, Professor T. Takabatake, Dr. T. Onimaru of Hiroshima University, and Professor K. Tanaka of Kyoto University for providing the clathrate samples. T.K. also acknowledges financial support by MEXT KAKENHI on the Priority Areas “New Materials Science Using Regulated Nano Spaces-Strategy in Ubiquitous Elements” and by the Advanced Low Carbon Technology Research Project and Development Program (ALCA) of the Japan Science and Technology Agency (JST).

- 3) T. N. Theis and P. M. Solomon, *Science* **327**, 1600 (2010).
- 4) M. Fujita, *Nat. Photonics* **7**, 264 (2013).
- 5) J. S. Kasper and S. M. Richards, *Acta Crystallogr.* **17**, 752 (1964).
- 6) R. H. Wentorf and J. S. Kasper, *Science* **139**, 338 (1963).
- 7) J. Weber and M. I. Alonso, *Phys. Rev. B* **40**, 5683 (1989).
- 8) M. d’Avezac, J.-W. Luo, T. Chanier, and A. Zunger, *Phys. Rev. Lett.* **108**, 027401 (2012).
- 9) A. G. Norman, J. M. Olson, J. F. Geisz, H. R. Moutinho, A. Mason, M. M. Al-Jassim, and S. M. Vernon, *Appl. Phys. Lett.* **74**, 1382 (1999).
- 10) K. Moriguchi, S. Munetoh, and A. Shintani, *Phys. Rev. B* **62**, 7138 (2000).
- 11) S. Botti, J. A. Flores-Livas, M. Amsler, S. Goedecker, and M. A. L. Marques, *Phys. Rev. B* **86**, 121204(R) (2012).
- 12) J. Noffsinger, E. Kioupakis, C. G. Van de Walle, S. G. Louie, and M. L. Cohen, *Phys. Rev. Lett.* **108**, 167402 (2012).
- 13) A. Bautista-Hernández, T. Rangel, A. H. Romero, G.-M. Rignanese, M. Salazar-Villanueva, and E. Chigo-Anota, *J. Appl. Phys.* **113**, 193504 (2013).
- 14) H. J. Xiang, B. Huang, E. Kan, S.-H. Wei, and X. G. Gong, *Phys. Rev. Lett.* **110**, 118702 (2013).
- 15) E. Y. Tonkov and E. G. Ponyatovsky, *Phase Transformations of Elements under High Pressure* (CRC Press, Boca Raton, FL, 2005) p. 96.
- 16) B. D. Malone, J. D. Sau, and M. L. Cohen, *Phys. Rev. B* **78**, 035210 (2008).
- 17) J. M. Besson, E. H. Mokhtari, J. Gonzalez, and G. Weill, *Phys. Rev. Lett.* **59**, 473 (1987).
- 18) J. Gryko, P. F. McMillan, R. F. Marzke, G. K. Ramachandran, D. Patton, S. K. Deb, and O. F. Sankey, *Phys. Rev. B* **62**, R7707 (2000).
- 19) H. V. Schnering, M. Schwarz, and R. Nesper, *J. Less-Common Met.* **137**, 297 (1988).
- 20) J. Dong, O. F. Sankey, and G. Kern, *Phys. Rev. B* **60**, 950 (1999).
- 21) A. M. Guloy, R. Ramlau, Z. Tang, W. Schnelle, M. Baitinger, and Y. A. Grin, *Nature* **443**, 320 (2006).
- 22) J. L. Cohn, G. S. Nolas, V. Fessatidis, T. H. Metcalf, and G. A. Slack, *Phys. Rev. Lett.* **82**, 779 (1999).
- 23) M. Christensen, A. B. Abrahamsen, N. B. Christensen, F. Juranyi, N. H. Andersen, K. Lefmann, J. Andreasson, C. R. H. Bahl, and B. B. Iversen, *Nat. Mater.* **7**, 811 (2008).
- 24) D. Connétable, V. Timoshevskii, B. Masenelli, J. Beille, J. Marcus, B. Barbara, A. M. Saitta, G.-M. Rignanese, P. Mélinon, S. Yamanaka, and X. Blase, *Phys. Rev. Lett.* **91**, 247001 (2003).
- 25) S. Yamanaka, E. Enishi, H. Fukuoka, and M. Yasukawa, *Inorg. Chem.* **39**, 56 (2000).
- 26) D. Y. Kim, S. Stefanoski, O. O. Kurakevych, and T. A. Strobel, *Nat. Mater.* **14**, 169 (2015).
- 27) O. O. Kurakevych, T. A. Strobel, D. Y. Kim, T. Muramatsu, and V. V. Struzhkin, *Cryst. Growth Des.* **13**, 303 (2013).
- 28) S. Yamanaka and S. Maekawa, *Z. Naturforsch.* **61**, 1493 (2006).
- 29) A. Wosylus, Y. Prots, U. Burkhardt, W. Schnelle, U. Schwarz, and Y. Grin, *Z. Naturforsch.* **61**, 1485 (2006).
- 30) A. Wosylus, Y. Prots, U. Burkhardt, W. Schnelle, and U. Schwarz, *Sci. Technol. Adv. Mater.* **8**, 383 (2007).
- 31) A. Wosylus, Y. Prots, U. Burkhardt, W. Schnelle, U. Schwarz, and Y. Grin, *Solid State Sci.* **8**, 773 (2006).
- 32) P. Hohenberg and W. Kohn, *Phys. Rev.* **136**, B864 (1964).
- 33) W. Kohn and L. J. Sham, *Phys. Rev.* **140**, A1133 (1965).
- 34) J. P. Perdew, J. A. Chevary, S. H. Vosko, K. A. Jackson, M. R. Pederson, D. J. Singh, and C. Fiolhais, *Phys. Rev. B* **46**, 6671 (1992).
- 35) J. P. Perdew, K. Burke, and M. Ernzerhof, *Phys. Rev. Lett.* **77**, 3865 (1996).
- 36) G. Kresse and J. Furthmüller, *J. Comput. Mater. Sci.* **6**, 15 (1996).
- 37) E. E. Salpeter and H. A. A. Bethe, *Phys. Rev.* **84**, 1232 (1951).
- 38) S. Albrecht, L. Reining, R. D. Sol, and G. Onida, *Phys. Rev. Lett.* **80**, 4510 (1998).
- 39) X. Gonze, B. Amadon, P.-M. Anglade, J.-M. Beuken, F. Bottin, P. Boulanger, F. Bruneval, D. Caliste, R. Caracas, M. Côté, T. Deutsch, L. Genovese, Ph. Ghosez, M. Giantomassi, S. Goedecker, D. R. Hamann, P. Hermet, F. Jollet, G. Jomard, S. Leroux, M. Mancini, S. Mazevet, M. J. T. Oliveira, G. Onida, Y. Pouillon, T. Rangel, G.-M. Rignanese, D. Sangalli, R. Shaltaf, M. Torrent, M. J. Verstraete, G. Zerah, and J. W. Zwanziger, *Comput. Phys. Commun.* **180**, 2582 (2009).
- 40) S. Stefanoski, C. D. Malliakas, M. G. Kanatzidis, and G. S. Nolas, *Inorg. Chem.* **51**, 8686 (2012).
- 41) M. C. Gupta and A. L. Ruoff, *J. Appl. Phys.* **51**, 1072 (1980).
- 42) P. Lautenschlager, M. Garriga, S. Logothetidis, and M. Cardona, *Phys. Rev. B* **35**, 9174 (1987).
- 43) S. Bobev and S. C. Sevov, *J. Solid State Chem.* **153**, 92 (2000).
- 44) K. A. Kovnir and A. V. Shevelkov, *Russ. Chem. Rev.* **73**, 923 (2004).
- 45) M. Beekman and G. S. Nolas, *J. Mater. Chem.* **18**, 842 (2008).
- 46) G. K. Ramachandran, J. Dong, J. Diefenbacher, J. Gryko, R. F. Marzke,

1) C. Kittel, *Introduction to Solid State Physics* (Wiley, New York, 2004) Chap. 3.

2) W. L. Ng, M. A. Lourenço, R. M. Gwilliam, S. Ledain, G. Shao, and K. P. Homewood, *Nature* **410**, 192 (2001).

- O. F. Sankey, and P. F. McMillan, *J. Solid State Chem.* **145**, 716 (1999).
- 47) E. D. Sloan, *Clathrate Hydrates of Natural Gases* (Marcel Dekker, New York, 1988) 2nd ed.
- 48) E. D. Sloan, *Nature* **426**, 353 (2003).
- 49) K. Umeo, M. A. Avila, T. Sakata, K. Suekuni, and T. Takabatake, *J. Phys. Soc. Jpn.* **74**, 2145 (2005).
- 50) M. A. Avila, K. Suekuni, K. Umeo, and T. Takabatake, *Physica B* **383**, 124 (2006).
- 51) H. Fukuoka, J. Kiyoto, and S. Yamanaka, *J. Solid State Chem.* **175**, 237 (2003).
- 52) W. C. Carrillo-Cabrera, S. Budnyk, Y. Prots, and Y. Grin, *Z. Anorg. Allg. Chem.* **630**, 2267 (2004).
- 53) N. L. Okamoto, K. Tanaka, and H. Inui, *Acta Mater.* **54**, 173 (2006).
- 54) H. Fukuoka, K. Iwai, S. Yamanaka, H. Abe, K. Yoza, and L. Haming, *J. Solid State Chem.* **151**, 117 (2000).
- 55) H. Fukuoka, K. Ueno, and S. Yamanaka, *J. Organomet. Chem.* **611**, 543 (2000).
- 56) K. Kishimoto, N. Ikeda, K. Akai, and T. Koyanagi, *Appl. Phys. Express* **1**, 031201 (2008).
- 57) T. Kume, S. Ohno, S. Sasaki, H. Shimizu, Y. Ohishi, N. L. Okamoto, K. Kishida, K. Tanaka, and H. Inui, *J. Appl. Phys.* **107**, 013517 (2010).
- 58) H. Shimizu, T. Iitaka, T. Fukushima, T. Kume, S. Sasaki, N. Sata, Y. Ohishi, H. Fukuoka, and S. Yamanaka, *J. Appl. Phys.* **101**, 063549 (2007).
- 59) A. San-Miguel, P. Kéghélian, X. Blase, P. Mélinon, A. Perez, J. P. Itié, A. Polian, E. Reny, C. Cros, and M. Pouchard, *Phys. Rev. Lett.* **83**, 5290 (1999).
- 60) H. Katzke, U. Bismayer, and P. Tolédano, *Phys. Rev. B* **73**, 134105 (2006).
- 61) A. San-Miguel and P. Toulemonde, *High Pressure Res.* **25**, 159 (2005).
- 62) A. San-Miguel, P. Mélinon, D. Connétable, X. Blase, F. Tourmus, E. Reny, S. Yamanaka, and J. P. Itié, *Phys. Rev. B* **65**, 054109 (2002).
- 63) A. San Miguel, A. Merlen, P. Toulemonde, T. Kume, S. Le Floch, A. Aouizerat, S. Pascarelli, G. Aquilanti, O. Mathon, T. Le Bihan, J.-P. Itié, and S. Yamanaka, *Europhys. Lett.* **69**, 556 (2005).
- 64) T. Kume, H. Fukuoka, T. Koda, S. Sasaki, H. Shimizu, and S. Yamanaka, *Phys. Rev. Lett.* **90**, 155503 (2003).
- 65) L. Yang, Y. M. Ma, T. Iitaka, J. S. Tse, K. Stahl, Y. Ohishi, Y. Wang, R. W. Zhang, J. F. Liu, H.-K. Mao, and J. Z. Jiang, *Phys. Rev. B* **74**, 245209 (2006).
- 66) J. S. Tse, R. Flacau, S. Desgreniers, T. Iitaka, and J. Z. Jiang, *Phys. Rev. B* **76**, 174109 (2007).
- 67) J. S. Tse, L. Yang, S. J. Zhang, C. Q. Jin, Ch. J. Sahle, C. Sternemann, A. Nyrow, V. Giordano, J. Z. Jiang, S. Yamanaka, S. Desgreniers, and C. A. Tulk, *Phys. Rev. B* **84**, 184105 (2011).
- 68) H. Shimizu, T. Kume, T. Kuroda, S. Sasaki, H. Fukuoka, and S. Yamanaka, *Phys. Rev. B* **71**, 094108 (2005).
- 69) J. S. Tse, S. Desgreniers, Z. Li, M. R. Ferguson, and Y. Kawazoe, *Phys. Rev. Lett.* **89**, 195507 (2002).
- 70) T. Kume, T. Koda, S. Sasaki, H. Shimizu, and J. S. Tse, *Phys. Rev. B* **70**, 052101 (2004).
- 71) D. Machon, P. Toulemonde, P. F. McMillan, M. Amboage, A. Muñoz, P. Rodríguez-Hernández, and A. San Miguel, *Phys. Rev. B* **79**, 184101 (2009).
- 72) H. Shimizu, T. Kume, T. Kuroda, S. Sasaki, H. Fukuoka, and S. Yamanaka, *Phys. Rev. B* **68**, 212102 (2003).
- 73) Y. Imaeda, T. Kume, S. Sasaki, H. Shimizu, K. Kishimoto, N. Ikeda, and T. Koyanagi, *J. Phys.: Conf. Ser.* **377**, 012037 (2012).
- 74) T. Kume, S. Sasaki, and H. Shimizu, *J. Phys. Chem. Solids* **71**, 583 (2010).
- 75) T. Onimaru, S. Tsutsui, M. Mizumaki, N. Kawamura, N. Ishimatsu, M. A. Avila, S. Yamamoto, H. Yamane, K. Suekuni, K. Umeo, T. Kume, S. Nakano, and T. Takabatake, *J. Phys. Soc. Jpn.* **83**, 013701 (2014).
- 76) H. Shimizu, T. Fukushima, T. Kume, S. Sasaki, H. Fukuoka, and S. Yamanaka, *J. Appl. Phys.* **101**, 113531 (2007).
- 77) T. Imai, T. Kume, S. Sasaki, H. Shimizu, A. Kaltzoglou, and T. F. Fässler, *J. Phys. Chem. Solids* **71**, 587 (2010).
- 78) T. Sukemura, T. Kume, T. Matsuoka, S. Sasaki, T. Onimaru, and T. Takabatake, *J. Phys.: Conf. Ser.* **500**, 182022 (2014).
- 79) M. I. McMahon, R. J. Nelmes, N. G. Wright, and D. R. Allan, *Phys. Rev. B* **50**, 739 (1994).
- 80) C. S. Menoni, J. Z. Hu, and I. L. Spain, *Phys. Rev. B* **34**, 362 (1986).
- 81) S. Nakano, *Koatsuryoku no Kagaku to Gijutsu* **22**, 26 (2012) [in Japanese].